Available online at www.sciencedirect.com

ScienceDirect

Journal of the Franklin Institute 356 (2019) 4577–4600

www.elsevier.com/locate/jfranklin

Neural dynamic sliding mode control of nonlinear systems with both matched and mismatched uncertainties

Ali Karami-Mollaee[a,*], Hamed Tirandaz[a], Oscar Barambones[b]

[a] *Electrical and Computer Engineering Faculty, Hakim Sabzevari University, Sabzevar, Iran*

[b] *Automatic Control and System Engineering Department, University of the Basque Country, UPV/EHU, Nieves Cano 12, Vitoria, Spain*

Received 10 June 2018; received in revised form 2 March 2019; accepted 11 April 2019

Available online 22 April 2019

Abstract

Mismatched uncertainty and chattering appear as two challenges in sliding mode control. To overcome the problem of mismatched uncertainty, multiple sliding surfaces with virtual inputs are proposed. Accordingly, we have proposed two new methods based on designed neural observer: sliding mode control (SMC) and dynamic sliding mode control (DSMC) methods. Although, the proposed SMC can significantly cope with the mismatched uncertainties, but it suffers from chattering phenomenon. The chattering problem can be removed in DSMC, because an integrator is placed before the system. This results in increased number of the system states. This new state can be identified with the proposed neural observer. Note that in both proposed approaches, the robust performance (invariance property) of system is reserved, even in the presence of mismatch uncertainties. Then, to have a valid comparison the proposed DSMC is also designed using loop transfer recovery observer (LTRO). This comparison shows the good performance of the DSMC based neural networks. Moreover, the upper bound of uncertainties is not used in SMC and DSMC controllers and also in the neural observer and LTRO, which is important in practical implementation. Finally, comparing the equations, one can see the simplicity of DSMC in concept and also in realization.

* Corresponding author.

E-mail address: karami@hsu.ac.ir (A. Karami-Mollaee).

https://doi.org/10.1016/j.jfranklin.2019.04.019

1. Introduction

Stability, performance and robustness of the practical systems are usually affected by uncertainties imposed to the system. To overcome structured uncertainties and disturbances, researchers use SMC due to its invariance property or robust performance. It is known that invariance is stronger than robustness, which is the main property of SMC method. However, invariance property of SMC method can be missed against mismatch uncertainty [1], where mismatch uncertainty would not affect the system directly in the input channel of the system. Some works are proposed to solve the effect of mismatch uncertainties [2–13]. However, the proposed solutions for this problem have some drawbacks. For example, in some works chattering is not removed because the Sign function is directly in the input control signal [2–19]. The works presented in [3,4] are complicated in concept and also in realization. Some works are devoted to linear systems, such as: [3,5]. In [3], a method is presented for linear systems based on LMI. In the works [6–8], the bound of uncertainty is used in the controller. The work of [9] is based on disturbance observer. In [10], sliding differentiator is utilized. Finally, in [1], an extended state observer is used. In [11], the effect of mismatched uncertainty is minimized and is based on LMI. In [12,13], multiple surfaces for SMC are used. Some other works are recently emphasized on this subject as [20–24]. In [20,21,25], the authors have supposed utilizing the boundedness of the disturbance derivative, which is the weakness of their works. In addition, the simulation results in [22] show that their proposed method has not good performance. Another work presented in [23] is devoted to the control designs of quadrotor dynamics with unknown dynamics and time-varying disturbances. The proposed approach is based on the terminal sliding mode. In the corresponding paper, the authors have not any concerns about chattering problem. Similarly, the approach presented in [24], which is devoted to the mismatched disturbance problem, does not discuss about the chattering phenomenon.

Unfortunately, another main drawback of SMC is chattering, which is defined as the small amplitude oscillations with high and finite frequency. Chattering can lead to some damages in electrical or mechanical parts of systems [26]. Four design methodologies have been proposed to solve this problem: boundary layer, adaptive boundary layer, higher order SMC (HOSMC) and DSMC [27]. Boundary layer and also adaptive boundary layer methods cannot preserve the invariance property of SMC [26–28]. HOSMC is proposed to reliably eliminate chattering [1,29]. In HOSMC, the effect of switching is totally eliminated by moving the switching to the higher order derivatives of the desired output [29]. Many algorithms are proposed for implementation of second or higher order SMC [30]. However, the main drawback is that the control methods generally require the knowledge of higher order derivatives of the plant model [30]. For example, if the relative degree is two, usually the plant model derivative would be estimated by means of some observer, for example sliding differentiator [31]. In DSMC, an integrator or any other strictly low-pass filter are placed before the input control signal of the plant [27]. Then, switching is removed from the input control signal, since the integrator filters the high frequency switching produced by SMC [27]. However, in DSMC the augmented system is one dimension bigger than the actual system. Therefore, the plant model should be completely known when one wants to use SMC to control the augmented system [27]. Therefore, in DSMC the plant model is needed but in HOSMC, the derivatives of plant model must be known. This is the main advantage of DSMC with respect to the HOSMC.

Therefore, to implement DSMC, we should identify the plant model. We know that system identification is an important issue in determining a dynamical model for an unknown plant.

System identification has been the focus of the attention by the researchers in the past several years [32–38]. Since neural networks can approximate any real continuous function with any arbitrary accuracy, which is known as universal approximation [39–41]. Therefore, neural networks have been widely employed for system identification [42–51]. Although neural networks based SMC are widely used to control of various systems. But, the problem of mismatch uncertainty is not considered in the past literature [47–51]. Moreover, neural networks have some prior properties such as online learning, adaptive learning and ability to deal with uncertainties [41]. These properties make them a reliable choice for model identification and state estimation of linear [52] or nonlinear systems [41]. These properties are our motivation to solve the problem of sliding surface estimation in DSMC and utilizing of a neural observer. This observer estimates the unknown part of the sliding surfaces.

Motivated by the above discussion, the aim of this paper is to control a nonlinear system using DSMC. We show that in DSMC, the system with both matched and mismatched uncertainties can be controlled properly, using appropriate definition of the multiple sliding surfaces and input control signal. The proposed method has some advantages than other investigated approaches. The chattering is removed in the proposed method. Moreover, a new neural observer is proposed, which can be utilized to estimate the system model and also its dynamics. The stability of the proposed observer is proved using Lyapunov stability theory, and also, the invariance property is maintained even in the existence of mismatched uncertainty. Another advantage of the proposed approach is its simplicity in concept and design. Furthermore, the upper bound of the uncertainties is not used in DSMC and neural observer, which is important from implementation point of view. In order to illustrate the advantages of the proposed approach, it is implemented with the SMC and DSMC using the same neural observer. Finally, to show the good performance of the neural observer, the proposed DSMC is implemented using loop transfer recovery observer (LTRO). With this comparison one can see the limitations of the LTRO with respect to the neural networks.

The reminder structure of the paper is as follows: In Section 2, some preliminaries background and problem formulations are defined. In Section 3, the structure of the proposed neural observer is presented. Section 4 and Section 5 are devoted to the design of control variables using SMC and DSMC, respectively. In Section 6 the comparison is illustrated using LTRO instead of neural network. Section 7, provides some numerical simulation results. Finally, some concluding remarks are given in Section 8.

2. Problem formulation

Without loss of generality, consider a class of second order systems as follows.

$$\begin{aligned} \dot{x}_1 &= x_2 + g_1(x,t) \\ \dot{x}_2 &= v + g_2(x,t) \\ y &= x_1 \\ x &= [x_1, x_2]^T \end{aligned} \tag{1}$$

Such that x is the accessible system state vector, v is the control signal and the functions $g_1(x, t)$ and $g_2(x, t)$ are unknown mismatched and unknown matched uncertainties, respectively, and y is the output of the system. The purpose is to control the system using SMC/DSMC with design of v in order to obtain the convergence of $y = x_1$ to zero even in the presence of $g_1(x, t)$ and $g_2(x, t)$ such that invariance property is also reserved. As we mentioned before, since

the system contains mismatched uncertainty, traditional SMC cannot be used. To solve this problem, a new strategy is proposed.

Considering to the first part of Eq. (1):

$$\dot{x}_1 = x_2 + g_1(x,t) \tag{2}$$

In the first step, we can consider the state x_2 as the virtual input control signal of the system Eq. (2) and thereafter, we calculate a reference signal for the state x_2 called x_{d2} in order to obtain that $y = x_1$ converges to zero using SMC/DSMC. In this case uncertainty g_1 is matched with respect to the x_2.

Now considering the second part of Eq. (1):

$$\dot{x}_2 = v + g_2(x,t) \tag{3}$$

In the second step, the aim is to calculate a input control signal v such that the state x_2 tracks the desired value x_{d2} obtained from the first step.

At first, the following state feedback is applied to the system Eq. (1).

$$v = -a_1 x_1 - a_2 x_2 + u \tag{4}$$

Then, system Eq. (1) can be rewritten as follows:

$$\dot{x} = Ax + Bu + g \tag{5}$$

where:

$$A = \begin{bmatrix} 0 & 1 \\ -a_1 & -a_2 \end{bmatrix}, B = \begin{bmatrix} 0 \\ 1 \end{bmatrix}, \; g = \begin{bmatrix} g_1 \\ g_2 \end{bmatrix}, x = \begin{bmatrix} x_1 \\ x_2 \end{bmatrix} \tag{6}$$

In which, constants a_1 and a_2 are chosen such that matrix A would be Hurwitz i.e. for any symmetric positive definite matrix A, there exists a symmetric positive definite matrix P satisfying Lyapunov equation.

$$A^T P + PA = -Q \tag{7}$$

3. The proposed neural observer

According to the universal approximation property of neural network theory [20], there exist some weights w such that a continuous vector function $g(x, t)$ can be represented as:

$$g(x,t) = w\sigma(\bar{x}) + \varepsilon(x) \tag{8}$$

Such that:

$$\bar{x} = [x^T, t]^T = [x_1, x_2, t]^T, \sigma(\bar{x}) = [\sigma_1(\bar{x}), \sigma_2(\bar{x}), \sigma_3(\bar{x})]^T, w \in R^{2\times 3}, \|\varepsilon(x)\| \le B_\varepsilon \tag{9}$$

where w is the unknown weight matrix, $\varepsilon(x)$ is the neural network bounded approximation error and $\sigma(\bar{x})$ is the transfer function of the hidden neurons that is usually considered as a Sigmoidal function.

$$\sigma_i(\bar{x}) = \frac{2}{1+\exp[-2M_i\bar{x}]} - 1 : i = 1,2,3$$
$$M_i = [m_1, m_2, m_3]$$
$$m_j = \begin{cases} 1 & : j = i \\ 0 & : j \neq i \end{cases} \tag{10}$$

Note that $\sigma_i(\bar{x})$ is the ith element of $\sigma(\bar{x})$. Hence, Eq. (5) can be expressed as:

$$\dot{x} = Ax + Bu + w\sigma(\bar{x}) + \varepsilon(x) \tag{11}$$

Moreover, the vector function g can be approximated as:

$$\hat{g} = \hat{w}\sigma(\bar{x}) \tag{12}$$

Therefore, the approximate model of system Eq. (5) can be written as follows:

$$\dot{\hat{x}}(t) = A\hat{x} + Bu + \hat{w}\sigma(\bar{x}) \tag{13}$$

Then, from Eq. (5) and Eq. (8) one can write:

$$\dot{x} = Ax + Bu + w\sigma(\bar{x}) + \varepsilon(x) \tag{14}$$

We define the following identification error:

$$\begin{aligned} \tilde{x} &= x - \hat{x} \\ \tilde{w} &= w - \hat{w} \end{aligned} \tag{15}$$

Now, subtracting Eq. (13) from Eq. (14) follows that:

$$\dot{\tilde{x}}(t) = A\tilde{x} + \tilde{w}\sigma(\bar{x}) + \varepsilon(x) \tag{16}$$

Theorem 1. *The error $\tilde{x} = x - \hat{x}$ converges to zero if the adaptive weight vector is updated according to:*

$$\dot{\hat{w}} = \eta(\tilde{x}^T A^{-1})^T(\sigma(\bar{x}))^T - \rho\,\|\tilde{x}\|\,\hat{w} \tag{17}$$

with arbitrary scalar constants $\eta > 0$ and $\rho > 0$.

Proof. Consider a Lyapunov function candidate as:

$$V = \frac{1}{2}\tilde{x}^T P\tilde{x} + \frac{1}{2}tr(\tilde{w}^T\rho^{-1}\tilde{w}) \tag{18}$$

The time derivative of Eq. (18) is given by:

$$\dot{V} = \frac{1}{2}\dot{\tilde{x}}^T P\tilde{x} + \frac{1}{2}\tilde{x}^T P\dot{\tilde{x}} + tr(\tilde{w}^T\rho^{-1}\dot{\tilde{w}}) \tag{19}$$

where $\dot{\tilde{\omega}} = -\dot{\hat{\omega}}$, and by substituting Eqs. (7), (16), and (17) into Eq. (19), one gets:

$$\dot{V} = -\frac{1}{2}\tilde{x}^T Q\tilde{x} + \tilde{x}^T P(\tilde{w}\sigma(\bar{x}) + \omega + \varepsilon) + tr\left(-\tilde{w}^T F\,\tilde{x}\sigma^T + \tilde{w}^T\|\tilde{x}\|\,(w - \tilde{w})\right) \tag{20}$$

where:

$$F = \eta\,\rho^{-1}A^{-T} \tag{21}$$

Taking into account following inequalities:

$$\begin{aligned} &tr(\,\tilde{w}^T(w - \tilde{w})) \le B_w\|\tilde{w}\| - \|\tilde{w}\|^2 \\ &tr(\tilde{w}^T F\tilde{x}\sigma^T) \le B_\sigma\left\|\tilde{w}^T\right\|\,\|F\|\,\|\tilde{x}\,\| \end{aligned} \tag{22}$$

where B_w and B_σ are the bounds of neural network parameters:

$$\|w\| \le B_w,\ \ \|\sigma(\bar{x})\| \le B_\sigma \tag{23}$$

Therefore:

$$\dot{V} \leq -\frac{1}{2}\lambda_{\min}(Q)\|\tilde{x}\|^2 + \|\tilde{x}\|\,\|P\|\,(\|\tilde{w}\|B_\sigma + B_\varepsilon) + B_\sigma\|\tilde{w}\|\,\|F\|\,\|\tilde{x}\| + \left(B_w\|\tilde{w}\| - \|\tilde{w}\|^2\right)\|\tilde{x}\| \tag{24}$$

or:

$$\dot{V} \leq -\left(\frac{1}{2}\lambda_{\min}(Q)\right)\|\tilde{x}\|^2 + \left(\|P\|\,(B_wB_\sigma + B_\varepsilon) + B_\sigma B_w\|F\| - \left(\|\tilde{w}\|^2 - B_w\|\tilde{w}\|\right)\right)\|\tilde{x}\| \tag{25}$$

Now, $B_{\tilde{x}}$ is defined as follow:

$$B_{\tilde{x}} = \frac{(\,\|P\|\,(B_wB_\sigma + B_\varepsilon) + B_\sigma B_w\,\|F\|\,) + \frac{1}{4}B_w^2}{\frac{1}{2}\lambda_{\min}(Q)} \tag{26}$$

Therefore:

$$\dot{V}(t) \leq -\left(\frac{1}{2}\lambda_{\min}(Q)\right)(\,\|\tilde{x}\| - B_{\tilde{x}}\,)\,\|\tilde{x}\| - \left(\|\tilde{w}\| - \frac{1}{2}B_w\right)^2\|\tilde{x}\| \tag{27}$$

or:

$$\dot{V}(t) \leq -\left(\frac{1}{2}\lambda_{\min}(Q)\right)(\,\|\tilde{x}\| - B_{\tilde{x}}\,)\,\|\tilde{x}\| \tag{28}$$

Take $r(t) = \left(\frac{1}{2}\lambda_{\min}(Q)\right)(\,\|\tilde{x}\| - B_{\tilde{x}}\,)\,\|\tilde{x}\|$ and suppose $\|\tilde{x}\| > B_{\tilde{x}}$ then, one can write $\dot{V} \leq -r(t) \leq 0$. Integration from zero to t yields:

$$0 \leq \int_0^t r(\tau)d\tau \leq \int_0^t r(\tau)d\tau + V(t) \leq V(0) \tag{29}$$

when $t \to \infty$, the above integral exists and is less than or equal to $V(0)$. Since $V(0)$ is positive and finite, according to the Barbalat's lemma [27], one will have:

$$\lim_{t\to\infty} r(t) = \lim_{t\to\infty}\left(\frac{1}{2}\lambda_{\min}(Q)\right)(\,\|\tilde{x}\| - B_{\tilde{x}}\,)\,\|\tilde{x}\| = 0 \tag{30}$$

Since $\left(\frac{1}{2}\lambda_{\min}(Q)\right)$ is greater than zero, Eq. (30) implies decreasing $\|\tilde{x}\|$ until it becomes less than $B_{\tilde{x}}$. As a consequence $\lim_{t\to\infty}\|\tilde{x}\| \leq B_{\tilde{x}}$. This guarantees that $B_{\tilde{x}}$ is the upper bound of $\|\tilde{x}\|$. □

4. The proposed SMC

In this case, we define two sliding surfaces as follows:

$$s_1 = k_1x_1 + k_2\dot{x}_1 \tag{31}$$

$$s_2 = \lambda_1(x_2 - x_{d2}) \tag{32}$$

Theorem 2. *The following input signal $\dot{x}_{d2}$ causes the sliding surface s_1 converges to zero in finite time.*

$$\dot{x}_{d2} = -\left(C_1\dot{\hat{w}}\sigma + C_1\hat{w}\dot{\sigma}\right) - \frac{k_1}{k_2}\left(x_{d2} + C_1\hat{w}\sigma(\bar{x})\right) - \frac{h_1}{k_2}s_1 - \frac{h_2}{k_2}sign(s_1) \tag{33}$$

$h_1 > 0$ *and* $h_2 > 0$

Proof. The estimation of first sliding surface Eq. (31) is as:

$$s_1 = k_1\hat{x}_1 + k_2\dot{\hat{x}}_1 = k_1\hat{x}_1 + k_2\left(x_{d2} + C_1\hat{w}\sigma\right) \tag{34}$$

and its derivative is as follows:

$$\dot{s}_1 = k_1\dot{\hat{x}}_1 + k_2\left(\dot{x}_{d2} + C_1\dot{\hat{w}}\sigma + C_1\hat{w}\dot{\sigma}\right) \tag{35}$$

or:

$$\dot{s}_1 = k_1\left(x_{d2} + C_1\hat{w}\sigma(\bar{x})\right) + k_2\left(\dot{x}_{d2} + C_1\dot{\hat{w}}\sigma + C_1\hat{w}\dot{\sigma}\right) \tag{36}$$

Replacing $\dot{x}_{d2}$ from Eq. (33) into Eq. (36) follows that:

$$\dot{s}_1 = -h_1 sign(s_1) - h_2 s_1 \tag{37}$$

Consider the Lyapunov function $V_1 = 0.5{s_1}^2$. Then, $\dot{V}_1 = s_1\dot{s}_1$ and hence from Eq. (37) we have:

$$\dot{V}_1 = -h_1|s_1| - h_2{s_1}^2 \leq -h_1|s_1| \tag{38}$$

Then, $s_1\dot{s}_1 \leq -h_1|s_1|$. Now suppose that t_1 is the finite reaching time to the sliding surface s_1 i.e. $s_1(t_1) = 0$. Then, it is easy to show that $t_1 \leq \frac{|s_1(0)|}{h_1}$ [53]. □

Theorem 3. *The following input signal u causes the sliding surface s_2 converges to zero in finite time.*

$$u = -\left(C_2\hat{w}\sigma(\bar{x}) - \sum_{i=1}^{2} a_i\hat{x}_i - \dot{x}_{d2}\right) - \frac{h_1}{\lambda_1}s_2 - \frac{h_2}{\lambda_1}sign(s_2) \tag{39}$$

$h_1 > 0$ *and* $h_2 > 0$

Proof. First notice that the estimation of second sliding surface Eq. (32) is as:

$$s_2 = \lambda_1\left(\hat{x}_2 - x_{d2}\right) \tag{40}$$

and its derivative is as follows:

$$\dot{s}_2 = \lambda_1\left(\dot{\hat{x}}_2 - \dot{x}_{d2}\right) \tag{41}$$

or:

$$\dot{s}_2 = \lambda_1\left(u + C_2\hat{w}\sigma(\bar{x}) - \sum_{i=1}^{2} a_i\hat{x}_i - \dot{x}_{d2}\right) \tag{42}$$

Replacing u from Eq. (39) into Eq. (42) follows that:

$$\dot{s}_2 = -h_1 sign(s_2) - h_2 s_2 \tag{43}$$

Consider the Lyapunov function $V_2 = 0.5{s_2}^2$. Then, $\dot{V}_2 = s_2\dot{s}_2$ and hence from Eq. (43) we have:

$$\dot{V}_2 = -h_1|s_2| - h_2{s_2}^2 \leq -h_1|s_2| \tag{44}$$

Then, $s_2\dot{s}_2 \leq -h_1|s_2|$. Now suppose that t_2 is the finite reaching time to the sliding surface s_2 i.e. $s_2(t_2) = 0$. Then, it is easy to show that $t_2 \leq \frac{|s_2(0)|}{h_1}$ [53]. □

Remark 1. In the proposed SMC, the variable $\dot{x}_{d2}$ cannot be used in the sliding surface Eq. (32), since according to Eq. (33) this variable is discontinuous.

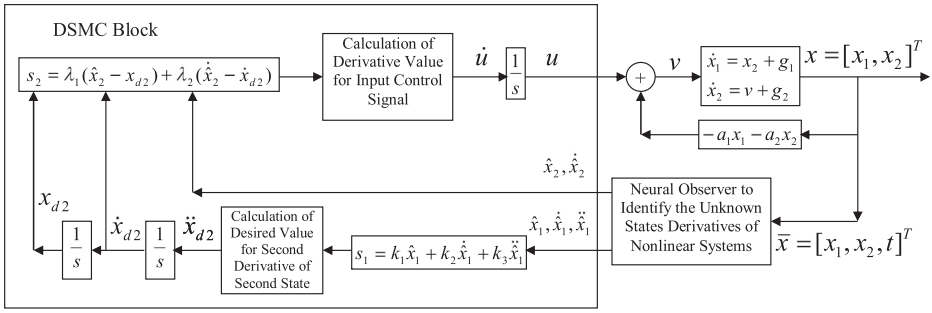

Fig. 1. The block diagram of the proposed DSMC method.

5. The proposed DSMC design

In this section, a new dynamic sliding mode controller is designed to suppress the chattering and to overcome the problem of mismatched uncertainty. Later, the effective performance of the proposed method is evaluated by comparison with the proposed sliding mode controller. The block diagram of the proposed DSMC method is presented in Fig. 1. In this diagram, as it can be seen, the position of the controller, the neural observer and the integrator blocks are clearly illustrated.

The presented observer in Eq. (13) is utilized in both controllers to have an appropriate comparison result. At first, to apply the proposed method, we write Eq. (13) into two parts as follows.

$$\dot{\hat{x}}_1(t) = x_{d2} + C_1\hat{w}\sigma(\bar{x}), C_1 = [1, 0] \tag{45}$$

$$\dot{\hat{x}}_2(t) = u + C_2\hat{w}\sigma(\bar{x}) - \sum_{i=1}^{2} a_i\hat{x}_i, C_2 = [0, 1] \tag{46}$$

Where x_{d2} is the desired value designed such that the output $y = x_1$ converges to zero. To this end, we define two sliding surfaces.

The first sliding surface can be defined as follows:

$$s_1 = kX_1,\ X_1 = [x_1, \dot{x}_1, \ddot{x}_1]^T,\ k = [k_1, k_2, k_3] \tag{47}$$

where X_1 converges to zero if s_1 becomes zero and the coefficients k_1, k_2, k_3 are properly chosen such that the polynomial $k_3S^2 + k_2S + k_1 = 0$ is Hurwitz.

Another sliding surface can be defined as follows:

$$s_2 = \lambda(X_2 - X_{d2}), X_2 = [x_2, \dot{x}_2]^T, X_{d2} = [x_{d2}, \dot{x}_{d2}]^T, \lambda = [\lambda_1, \lambda_2] \tag{48}$$

Again X_2 converges to X_{d2} if s_2 becomes zero and the coefficients λ_1, λ_2 are properly chosen such that the polynomial $\lambda_2S + \lambda_1 = 0$ is Hurwitz.

But, there is a problem for the calculation of these sliding surfaces. Only the state vector $x = [x_1, x_2]^T$ is accessible and the variables $\dot{x}_1, \ddot{x}_1, \dot{x}_2$ cannot be evaluated due to the unknown uncertainties g_1 and g_2. To solve this problem we used the proposed neural observer which is described in Section 3.

Theorem 4. *The following input signal $\ddot{x}_{d2}$ causes that the sliding surface s_1 converges to zero in finite time.*

$$\begin{aligned}\ddot{x}_{d2} = &-\left(C_1\dddot{\hat{w}}\sigma + C_1\ddot{\hat{w}}\dot{\sigma} + C_1\dot{\hat{w}}\ddot{\sigma} + C_1\hat{w}\dddot{\sigma}\right)\\ &-\frac{k_1}{k_3}\left(x_{d2} + C_1\hat{w}\sigma(\bar{x})\right) - \frac{k_2}{k_3}\left(\dot{x}_{d2} + C_1\ddot{\hat{w}}\sigma + C_1\dot{\hat{w}}\dot{\sigma}\right) - \frac{h_1}{k_3}s_1 - \frac{h_2}{k_3}sign(s_1)\\ &h_1 > 0 \ \ and \ \ h_2 > 0\end{aligned} \tag{49}$$

Proof. First notice that the estimation of first sliding surface Eq. (47) is:

$$s_1 = k_1\hat{x}_1 + k_2\dot{\hat{x}}_1 + k_3\ddot{\hat{x}}_1 = k_1\hat{x}_1 + k_2\left(x_{d2} + C_1\hat{w}\sigma\right) + k_3\left(\dot{x}_{d2} + C_1\dot{\hat{w}}\sigma + C_1\hat{w}\dot{\sigma}\right) \tag{50}$$

and its derivative is as follows:

$$\dot{s}_1 = k_1\dot{\hat{x}}_1 + k_2\left(\dot{x}_{d2} + C_1\dot{\hat{w}}\sigma + C_1\hat{w}\dot{\sigma}\right) + k_3\left(\ddot{x}_{d2} + C_1\ddot{\hat{w}}\sigma + C_1\dot{\hat{w}}\dot{\sigma} + C_1\dot{\hat{w}}\dot{\sigma} + C_1\hat{w}\ddot{\sigma}\right) \tag{51}$$

or using Eq. (45):

$$\begin{aligned}\dot{s}_1 = &\ k_1\left(x_{d2} + C_1\hat{w}\sigma(\bar{x})\right) + k_2\left(\dot{x}_{d2} + C_1\dot{\hat{w}}\sigma + C_1\hat{w}\dot{\sigma}\right)\\ &+ k_3\left(\ddot{x}_{d2} + C_1\ddot{\hat{w}}\sigma + C_1\dot{\hat{w}}\dot{\sigma} + C_1\dot{\hat{w}}\dot{\sigma} + C_1\hat{w}\ddot{\sigma}\right)\end{aligned} \tag{52}$$

Replacing $\ddot{x}_{d2}$ from Eq. (49) into Eq. (52) follows that:

$$\dot{s}_1 = -h_1 sign(s_1) - h_2 s_1 \tag{53}$$

Consider the Lyapunov function $V_1 = 0.5{s_1}^2$. Then, $\dot{V}_1 = s_1\dot{s}_1$ and hence from Eq. (53) we have:

$$\dot{V}_1 = -h_1|s_1| - h_2{s_1}^2 \le -h_1|s_1| \tag{54}$$

Accordingly $s_1\dot{s}_1 \le -h_1|s_1|$. Now suppose that t_1 is the finite reaching time to the sliding surface s_1 i.e. $s_1(t_1) = 0$. Then it is easy to show that $t_1 \le \frac{|s_1(0)|}{h_1}$ [53]. □

Theorem 5. *The following input signal $\dot{u}$ causes that the sliding surface s_2 converges to zero in finite time.*

$$\begin{aligned}\dot{u} = &-\frac{\lambda_1}{\lambda_2}\left(u + C_2\hat{w}\sigma(\bar{x}) - \sum_{i=1}^{2} a_i\dot{\hat{x}}_i - \dot{x}_{d2}\right)\\ &-\left(C_2\dddot{\hat{w}}\sigma + C_2\ddot{\hat{w}}\dot{\sigma} - a_1\left(x_{d2} + C_1\hat{w}\sigma(\bar{x})\right) - a_2\left(u + C_2\hat{w}\sigma(\bar{x}) - \sum_{i=1}^{2} a_i\dot{\hat{x}}_i\right) - \ddot{x}_{d2}\right)\\ &-\frac{h_1}{\lambda_2}s_2 - \frac{h_2}{\lambda_2}sign(s_2)\\ &h_1 > 0 \ \ and \ \ h_2 > 0\end{aligned} \tag{55}$$

Proof. First notice that the estimation of second sliding surface Eq. (48) is:

$$\begin{aligned}s_2 &= \lambda_1\left(\hat{x}_2 - x_{d2}\right) + \lambda_2\left(\dot{\hat{x}}_2 - \dot{x}_{d2}\right)\\ &= \lambda_1\left(\hat{x}_2 - x_{d2}\right) + \lambda_2\left(u + C_2\hat{w}\sigma - \sum_{i=1}^{2} a_i\dot{\hat{x}}_i - \dot{x}_{d2}\right)\end{aligned} \tag{56}$$

and its derivative is as follows:

$$\dot{s}_2 = \lambda_1\left(\dot{\hat{x}}_2 - \dot{x}_{d2}\right) + \lambda_2\left(\dot{u} + C_2\dot{\hat{w}}\sigma + C_2\hat{w}\dot{\sigma} - a_1\dot{\hat{x}}_1 - a_2\dot{\hat{x}}_2 - \ddot{x}_{d2}\right) \tag{57}$$

or:

$$\begin{aligned}\dot{s}_2 = {} & \lambda_1\left(u + C_2\hat{w}\sigma(\bar{x}) - \sum_{i=1}^{2} a_i\hat{x}_i - \dot{x}_{d2}\right) \\ & + \lambda_2\left(\dot{u} + C_2\dot{\hat{w}}\sigma + C_2\hat{w}\dot{\sigma} - a_1\left(x_{d2} + C_1\hat{w}\sigma(\bar{x})\right)\right. \\ & \left. -a_2\left(u + C_2\hat{w}\sigma(\bar{x}) - \sum_{i=1}^{2} a_i\hat{x}_i\right) - \ddot{x}_{d2}\right)\end{aligned} \tag{58}$$

Replacing $\dot{u}$ from Eq. (55) into Eq. (58) follows that:

$$\dot{s}_2 = -h_1 sign(s_2) - h_2 s_2 \tag{59}$$

Consider the Lyapunov function $V_2 = 0.5{s_2}^2$. Then $\dot{V}_2 = s_2\dot{s}_2$ and hence from Eq. (59) we have:

$$\dot{V}_2 = -h_1|s_2| - h_2{s_2}^2 \leq -h_1|s_2| \tag{60}$$

Then $s_2\dot{s}_2 \leq -h_1|s_2|$. Now, suppose that t_2 is the finite reaching time to the sliding surface s_2 i.e. $s_2(t_2) = 0$. Then it is easy to show that $t_2 \leq \frac{|s_2(0)|}{h_1}$ [53]. □

Remark 2. Note that the Sign function that generates the discontinuity, appears in $\dot{u}$ and then due to the integral action, u is smooth and without chattering because the integration act as a low pass filter. The same result is true for $\ddot{x}_{d2}$ which is discontinuous but $\dot{x}_{d2}$ and x_{d2} are smooth. Therefore, the components of the sliding surface Eq. (56) are continuous and then it is a continuous function.

6. The DSMC design based proposed LTRO

To show the performance and preference of the proposed neural observer, another comparison is presented in this section using Loop Transfer Recovery Observer (LTRO) to implement DSMC. At first we rewrite Eq. (5) as follows:

$$\begin{aligned}\dot{X}_1 &= E_1X_1 + H_1(\ddot{x}_2 + \Delta_1) \\ \dot{X}_2 &= E_2X_2 + H_2(a_1a_2x_1 - a_1x_2 + {a_2}^2x_2 - a_2u + \dot{u} + \Delta_2)\end{aligned} \tag{61}$$

where X_1 and X_2 are defined in Eq. (47) and Eq. (48) and:

$$E_1 = \begin{bmatrix}0 & 1 & 0\\ 0 & 0 & 1\\ 0 & 0 & 0\end{bmatrix}, H_1 = \begin{bmatrix}0\\ 0\\ 1\end{bmatrix}, E_2 = \begin{bmatrix}0 & 1\\ 0 & 0\end{bmatrix}, H_2 = \begin{bmatrix}0\\ 1\end{bmatrix} \tag{62}$$

and $\Delta_i : \ i = 1, 2$ are the unknown uncertainties.

$$\Delta_1 = \ddot{g}_1(x,t),\ \Delta_2 = -a_1g_1(x,t) - a_2g_2(x,t) + \dot{g}_2(x,t) \tag{63}$$

For the dynamical systems (61) the following observer is suggested to estimate the vector $X_i : \ i = 1, 2$.

$$\begin{aligned}\dot{\hat{X}}_1 &= E_1\hat{X}_1 + H_1(\ddot{x}_{d2}) + L_1(x_1 - G_1\hat{X}_1)\\ \dot{\hat{X}}_2 &= E_2\hat{X}_2 + H_2(a_1a_2x_1 - a_1x_2 + {a_2}^2x_2 - a_2u + \dot{u}) + L_2(x_2 - G_2\hat{X}_2)\end{aligned} \tag{64}$$

where:

$$\begin{aligned}&L_i = P_i{G_i}^T/\mu\,,\ \mu > 0 : i = 1, 2\\ &G_1 = [1, 0, 0],\ G_2 = [1, 0]\end{aligned} \tag{65}$$

and moreover P_i will be calculated from the following Riccati equation.

$$(I_i + E_i)^T P_i + P_i(I_i + E_i) - P_i{G_i}^T G_iP_i/\mu + \phi P_i^{-1}H_i{H_i}^T{P_i}^{-1} = 0 : i = 1, 2 \tag{66}$$

which scalar $\phi > 0$ is sufficiently large enough and I_i is the identity matrix with appropriate dimension. Note that the first components of X_1 and X_2 are system states and are available but the other components are not.

Lemma 1. *Since $(E_i + I_i, H_i, G_i)$ is minimum-phase, the solution P_i of the observer Riccati Eq. (66) satisfies $\lim_{\phi\to\infty}(P_i/\phi) = 0 : i = 1, 2$ [56].*

Theorem 6. *The observer error $\tilde{X}_1 = X_1 - \hat{X}_1$ converges to zero.*

Proof. From Eq. (61) and Eq. (64) one can write:

$$\dot{\tilde{X}}_1 = (E_1 - L_1G_1)\tilde{X}_1 + H_1\,\Delta_1 + H_1(\ddot{x}_2 - \ddot{x}_{d2}) \tag{67}$$

Set the Lyapunov function $V_1 = {\tilde{X}_1}^T{P_1}^{-1}\tilde{X}_1$ for the error dynamic Eq. (67), and calculate its derivative.

$$\begin{aligned}\dot{V}_1 &= {\dot{\tilde{X}}_1}^T{P_1}^{-1}\tilde{X}_1 + {\tilde{X}_1}^T{P_1}^{-1}\dot{\tilde{X}}_1\\ &\le -2V_1 - \tfrac{1}{\mu}\left\|G_1P_1\tilde{X}_1\right\|^2 - \phi\left\|{H_1}^T{P_1}^{-1}\tilde{X}_1\right\|^2\\ &\quad +2(\|\Delta_1\| + \|\ddot{x}_2 - \ddot{x}_{d2}\|)\left\|{H_1}^T{P_1}^{-1}\tilde{X}_1\right\|\\ &\le -\left(\tfrac{1}{\mu}\|G_1P_1\|^2 + \phi\left\|{H_1}^T{P_1}^{-1}\right\|^2\right)\left\|\tilde{X}_1\right\|^2\\ &\quad +\left(\,2(\|\Delta_1\| + \|\ddot{x}_2 - \ddot{x}_{d2}\|)\left\|{H_1}^T{P_1}^{-1}\right\|\,\right)\left\|\tilde{X}_1\right\|\end{aligned} \tag{68}$$

Now, $B_{\tilde{X}}$ is defined as follow:

$$B_{\tilde{X}} = \frac{2(\|\Delta_1\| + \|\ddot{x}_2 - \ddot{x}_{d2}\|)\left\|{H_1}^T{P_1}^{-1}\right\|}{\tfrac{1}{\mu}\|G_1P_1\|^2 + \phi\left\|{H_1}^T{P_1}^{-1}\right\|^2} \tag{69}$$

Then:

$$\dot{V}_1 \le -\left(\frac{1}{\mu}\|G_1P_1\|^2 + \phi\left\|{H_1}^T{P_1}^{-1}\right\|^2\right)\left(\,\left\|\tilde{X}_1\right\| - B_{\tilde{X}}\,\right)\left\|\tilde{X}_1\right\| \tag{70}$$

Take $r(t) = (\tfrac{1}{\mu}\|G_1P_1\|^2 + \phi\|{H_1}^T{P_1}^{-1}\|^2)\,(\,\|\tilde{X}_1\| - B_{\tilde{X}}\,)\,\|\tilde{X}_1\|$ and suppose $\|\tilde{X}_1\| > B_{\tilde{X}}$ then we can obtain $\dot{V}_1 \le -r(t) \le 0$. Integrating from zero to t yields:

$$0 \le \int_0^t r(\tau)d\tau \le \int_0^t r(\tau)d\tau + V_1(t) \le\ V_1(0) \tag{71}$$

When $t \to \infty$, the above integral exists and is less than or equal to $V_1(0)$. Since $V_1(0)$ is positive and finite, according to Barbalat's lemma [53] we will have:

$$\lim_{t\to\infty} r(t) = \lim_{t\to\infty} \left(\frac{1}{\mu} \|G_1 P_1\|^2 + \phi \left\| H_1{}^T P_1{}^{-1} \right\|^2 \right) \left(\left\| \tilde{X}_1 \right\| - B_{\tilde{X}} \right) \left\| \tilde{X}_1 \right\| = 0 \tag{72}$$

Since $\left(\frac{1}{\mu} \|G_1 P_1\|^2 + \phi \left\| H_1{}^T P_1{}^{-1} \right\|^2 \right)$ is greater than zero, Eq. (72) implies decreasing $\left\| \tilde{X}_1 \right\|$ until it becomes less than $B_{\tilde{X}}$. Then, $\lim_{t\to\infty} \left\| \tilde{X}_1 \right\| \le B_{\tilde{X}}$ and this guarantees that $B_{\tilde{X}}$ is the upper bound of $\left\| \tilde{X}_1 \right\|$. □

Theorem 7. *The observer error $\tilde{X}_2 = X_2 - \hat{X}_2$ converges to zero.*

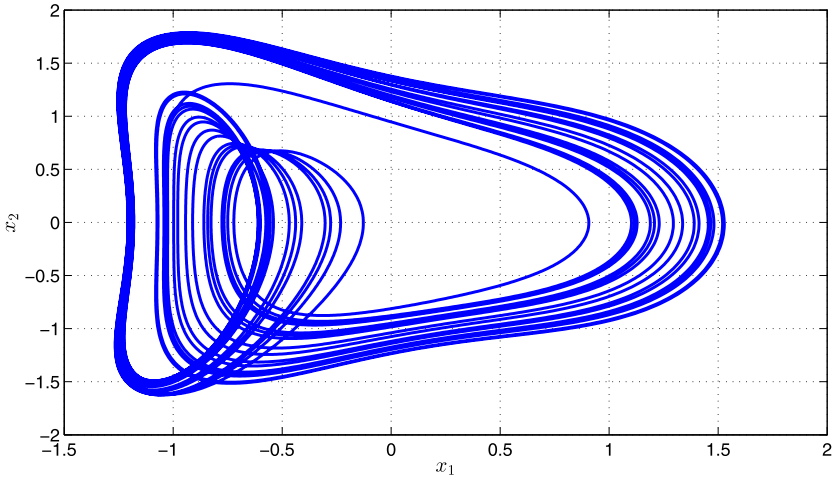

Fig. 2. The phase portrait of the improved Duffing–Holmes chaotic system.

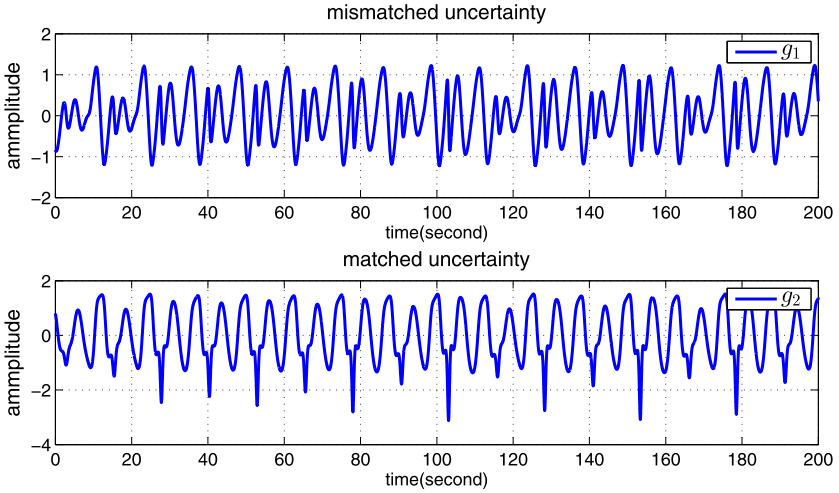

Fig. 3. The mismatched and matched uncertainties in the improved Duffing–Holmes chaotic system.

Proof. From Eq. (61) and Eq. (64) one can write:

$$\dot{\tilde{X}}_2 = (E_2 - L_2 G_2)\tilde{X}_2 + H_2\,\Delta_2 \tag{73}$$

Using the Lyapunov function $V_2 = \tilde{X_2}^T P_2^{-1} \tilde{X}_2$ results:

$$\dot{V}_2 \le -2V_2 - \frac{1}{\mu}\left\|G_2 P_2 \tilde{X}_2\right\|^2 - \phi\left\|H_2{}^T P_2^{-1}\tilde{X}_2\right\|^2 + 2(\|\Delta_2\|)\left\|H_2{}^T P_2^{-1}\tilde{X}_2\right\| \tag{74}$$

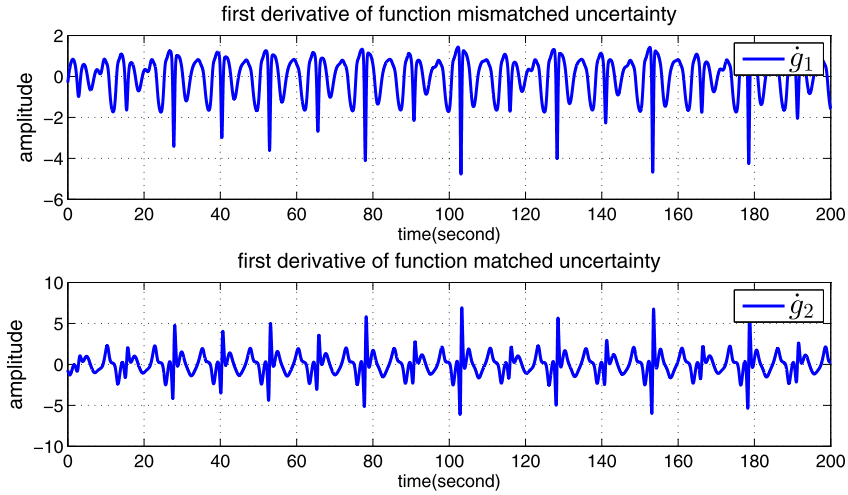

Fig. 4. The first derivative of mismatched and matched uncertainties in the improved Duffing–Holmes chaotic system.

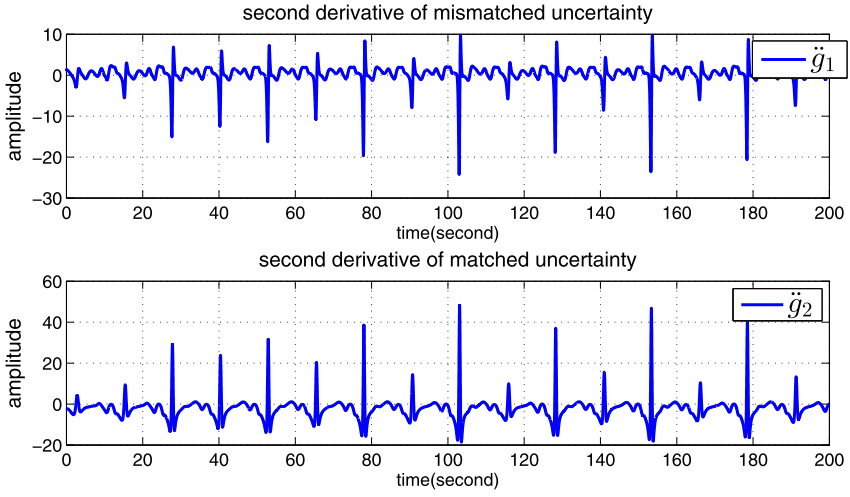

Fig. 5. The second derivative of mismatched and matched uncertainties in the improved Duffing–Holmes chaotic system.

The next procedure of the proof is as the Theorem 6. But the bound $B_{\tilde{X}}$ is defined as follows:

$$B_{\tilde{X}} = \frac{2\|\Delta_1\| \left\|H_2{}^T P_2{}^{-1}\right\|}{\frac{1}{\mu}\|G_2 P_2\|^2 + \phi \left\|H_2{}^T P_2{}^{-1}\right\|^2} \tag{75}$$

□

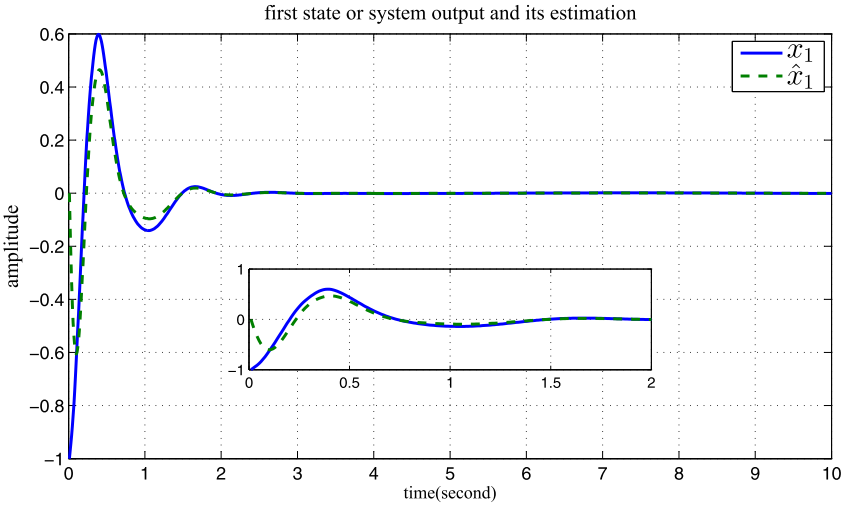

Fig. 6. First state or system output and its estimation in SMC based neural observer.

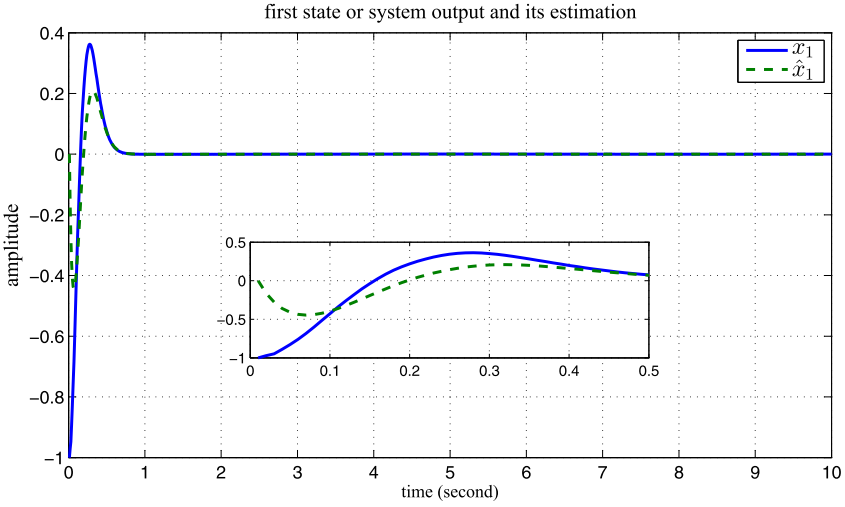

Fig. 7. First state or system output and its estimation in DSMC based neural observer.

Theorem 8. *The following dynamical equation causes the sliding surface s_1 defined in Eq. (47) converges to zero in finite time.*

$$\ddot{x}_{d2} = -(kH_1)^{-1}\Big(kE_1\hat{X}_1 + kL_1(x_1 - G_1\hat{X}_1) + h_1\, s_1 + h_2\, sign(s_1)\Big)$$
$$h_1 > 0 \;\; and \;\; h_2 > 0 \tag{76}$$

Proof. The proof of this theorem can be obtained using the Lyapunov function $V_1 = 0.5{s_1}^2$, and it is omitted here for its simplicity. □

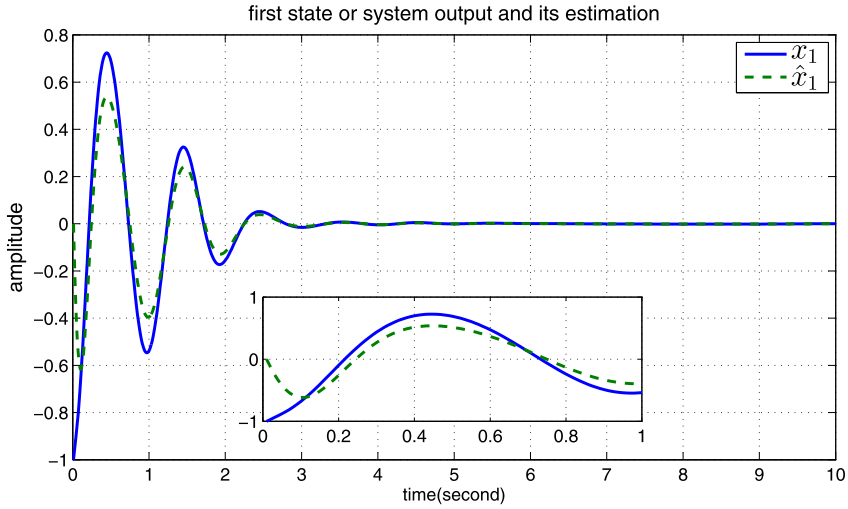

Fig. 8. First state or system output and its estimation in DSMC based LTRO.

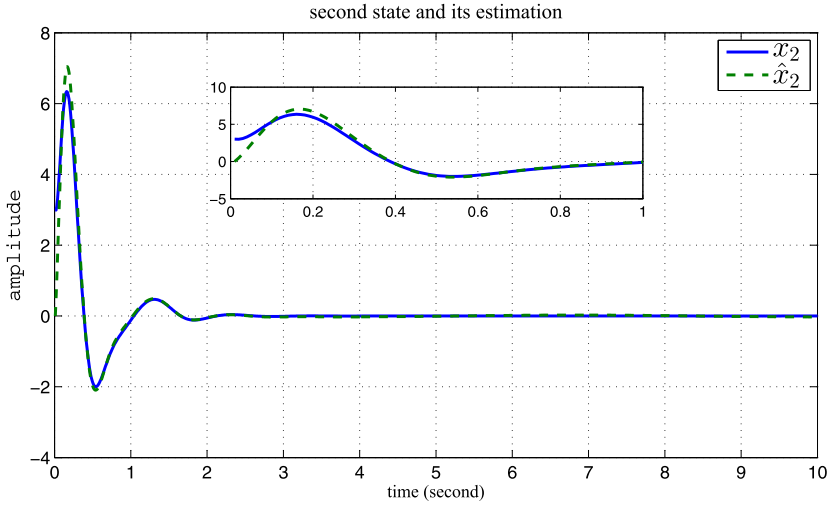

Fig. 9. Second state and its estimation in SMC based neural observer.

Theorem 9. *The following dynamical equation causes the sliding surface s_2 defined in Eq. (48) converges to zero in finite time.*

$$\begin{aligned}\dot{u} &= -(a_1a_2x_1 - a_1x_2 + {a_2}^2x_2 - a_2u) - (\lambda H_2)^{-1}\Big(\lambda E_2\hat{X}_2 + \lambda L_2(x_2 - G_2\hat{X}_2)\Big) \\ &\quad -(\lambda H_2)^{-1}\big(-\lambda\dot{X}_{d2} + h_1s_2 + h_2 sign(s_2)\big) \\ h_1 &> 0 \ \ and \ \ h_2 > 0\end{aligned} \tag{77}$$

Proof. The proof of this theorem can be obtained using the Lyapunov function $V_1 = 0.5{s_2}^2$, and it is omitted here for its simplicity. □

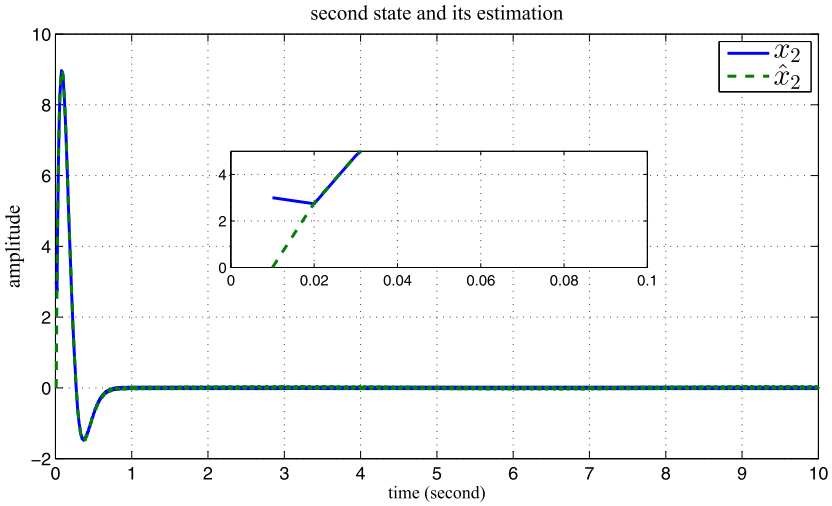

Fig. 10. Second state and its estimation in DSMC based neural observer.

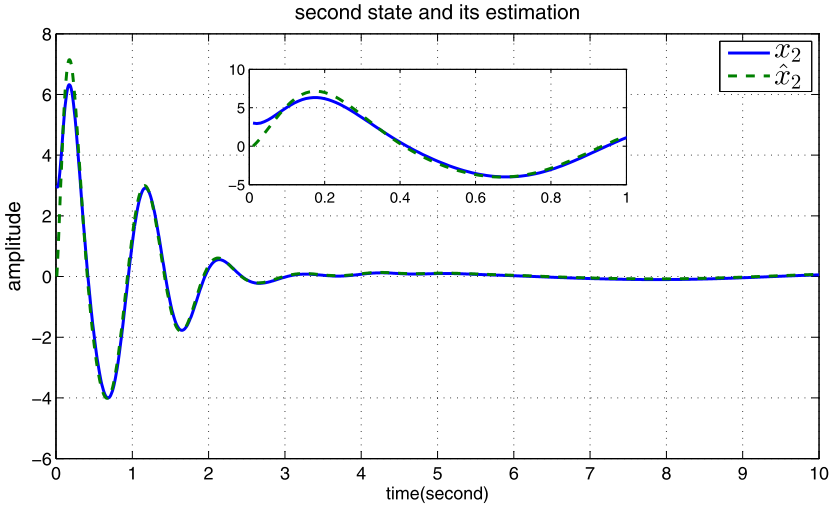

Fig. 11. Second state and its estimation in DSMC based LTRO.

7. Simulation results

As we mentioned before, the input control of the system u is calculated via SMC and DSMC such that the second state x_2 tracks the reference x_{d2} in both methods. As a result, x_{d2} caused that $y = x_1$ converges to zero while is invariant with respect to g_1 which is exactly the objective of this paper.

For comparison, the proposed approach is applied to the improved Duffing–Holmes chaotic system. The original Duffing–Holmes chaotic system which is used in [54,55] can be defined as follows:

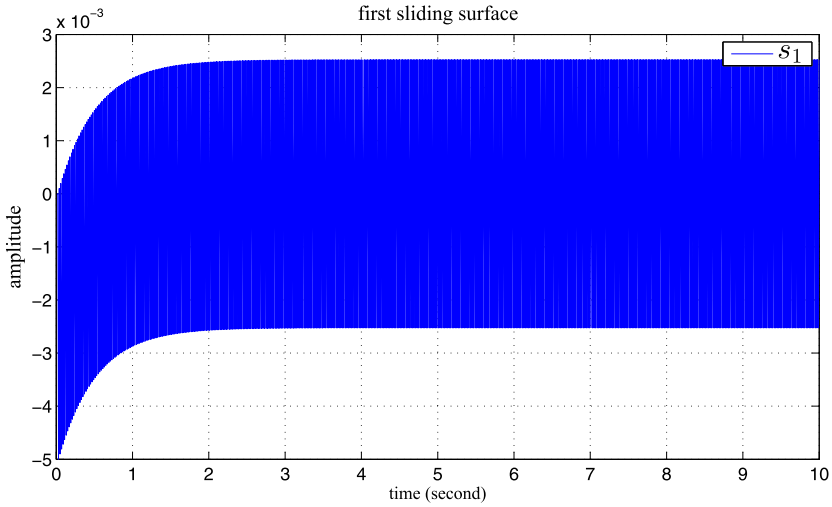

Fig. 12. First sliding surface in SMC based neural observer.

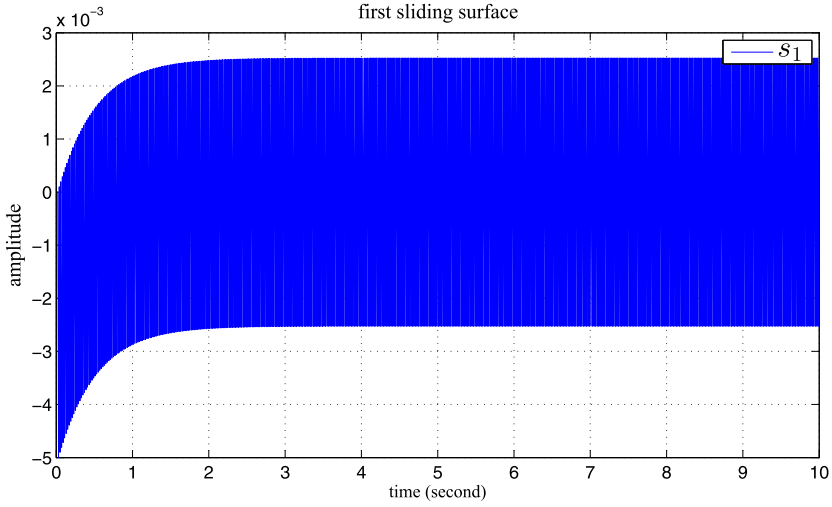

Fig. 13. First sliding surface in DSMC based neural observer.

$$\begin{aligned}\dot{x}_1 &= x_2\\ \dot{x}_2 &= x_1 - x_1^3 - 0.5x_2 + 1.3\cos(t) + v\\ y &= x_1\end{aligned} \tag{78}$$

To show the advantages of our method, we extend this system as follows:

$$\begin{aligned}\dot{x}_1 &= x_2 + g_1, \quad g_1(x,t) = x_1\sin(x_2)\\ \dot{x}_2 &= v + g_2, \quad g_2(x,t) = x_1 - x_1^3 - 0.5x_2 + 1.3\cos(t)\\ y &= x_1\end{aligned} \tag{79}$$

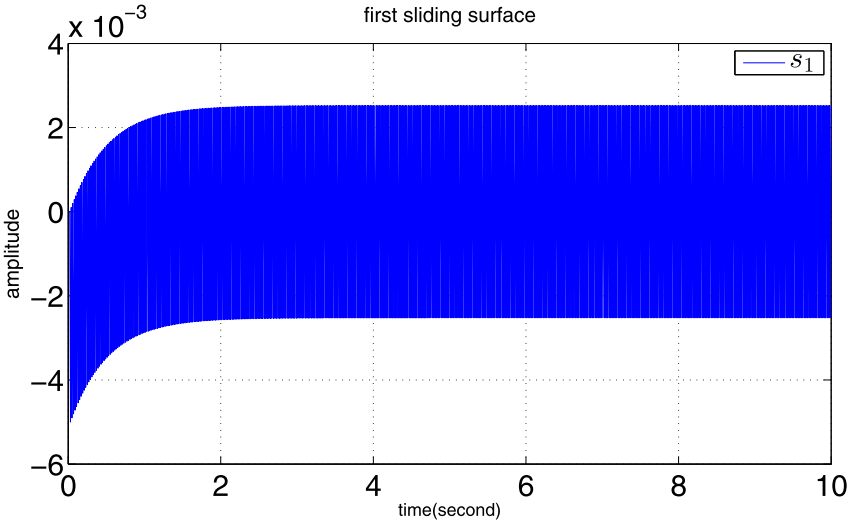

Fig. 14. First sliding surface in DSMC based LTRO.

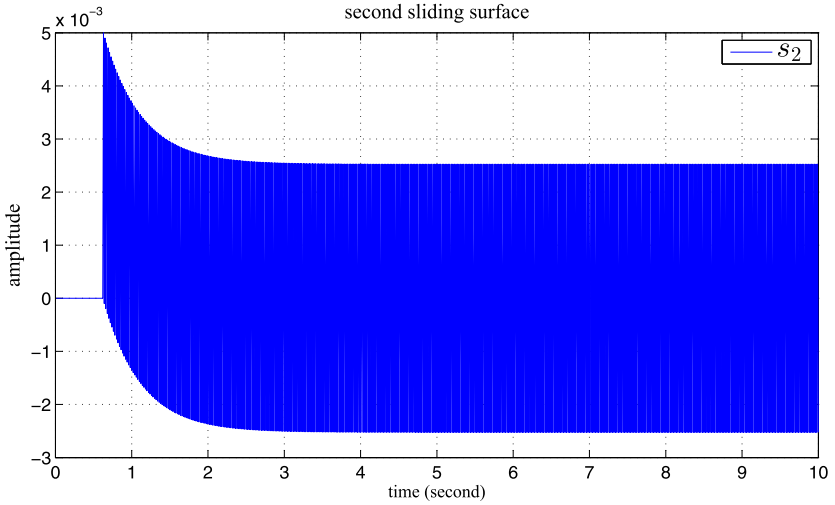

Fig. 15. Second sliding surface in SMC based neural observer.

The behavior of the improved Duffing–Holmes chaotic system represented in Eq. (79) are shown in Figs. 2–5.

We have done three simulations for comparison, using SMC and DSMC with the same neural observer and DSMC using LTRO. In SMC, the sliding coefficients parameters are selected as $k_1 = 1, k_2 = 0.1, \lambda_1 = 1$. Moreover, the parameters of the state feedback in Eq. (4) are set as $a_1 = 5, a_2 = 2$. Other design parameters are $h_1 = 2, h_2 = 0.5$ and the initial conditions of the system states are selected as $x_1(0) = -1, x_2(0) = 3$. Moreover, the initial conditions of the observer states are considered as $\hat{x}_1(0) = 0$, $\hat{x}_2(0) = 0$. Then, based on Eq. (26) to reduce the bound $B_{\tilde{x}}$, we select the matrix Q as follow such that $\lambda_{min}(Q)$ should

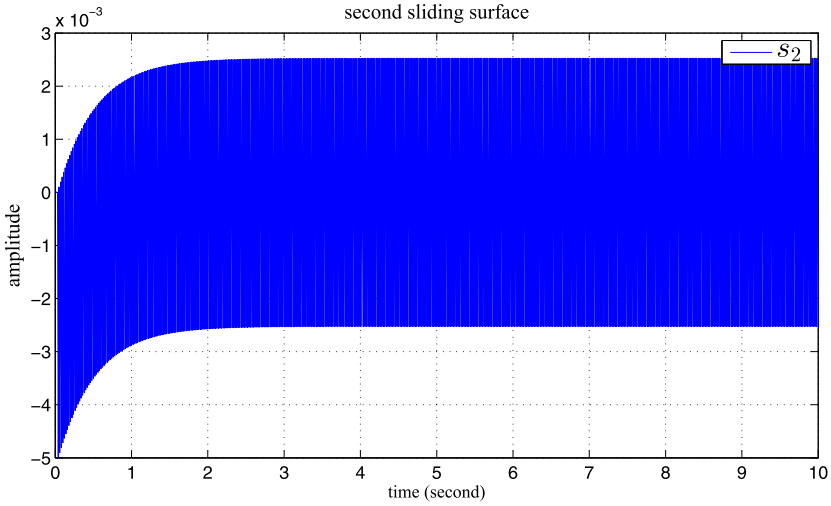

Fig. 16. Second sliding surface in DSMC based neural observer.

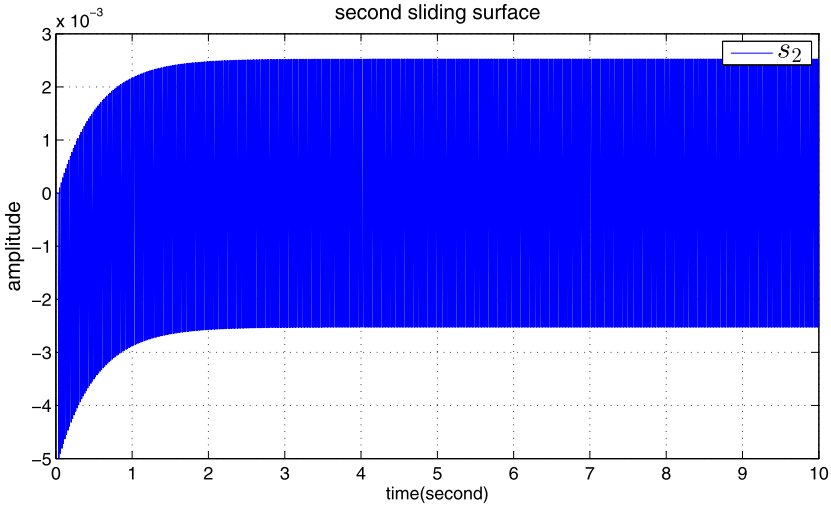

Fig. 17. Second sliding surface in DSMC based LTRO.

be large enough.

$$Q = \begin{bmatrix} 20 & 0 \\ 0 & 30 \end{bmatrix} \tag{80}$$

On the other hand, in DSMC based neural observer approach the parameters of sliding surfaces Eq. (47) and Eq. (48) are chosen as $k_1 = 10, k_2 = 1, k_3 = 0.1, \lambda_1 = 10, \lambda_2 = 1$. The other design parameters are set as before. Moreover, in DSMC based LTRO approach the parameters are chosen as $\phi = 10,000$ and $\mu = 1$ and the other design parameters are also set as before. To calculate the derivative of the input control signal $\dot{u}$, in DSMC approaches the initial value of u is needed which is set to zero i.e. $u(0) = 0$.

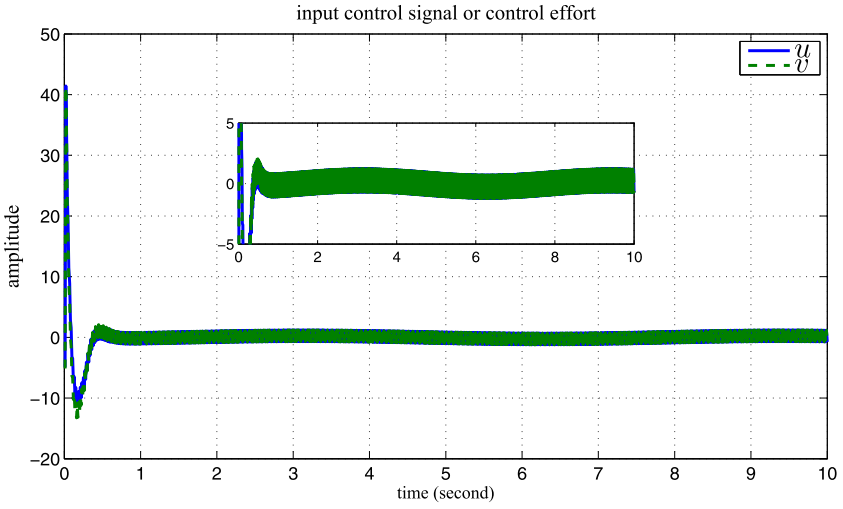

Fig. 18. Input control signal and its chattering in SMC based neural observer.

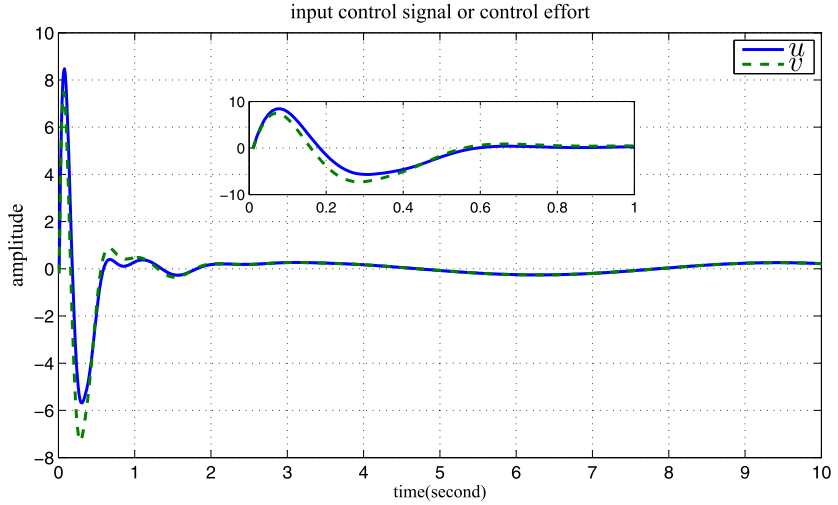

Fig. 19. Chattering-less input control signal in DSMC based neural observer.

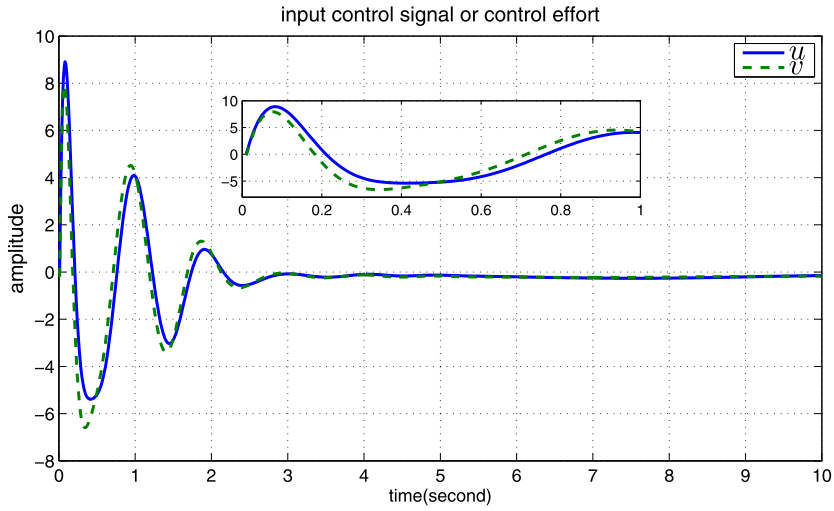

Fig. 20. Chattering-less input control signal in DSMC based LTRO.

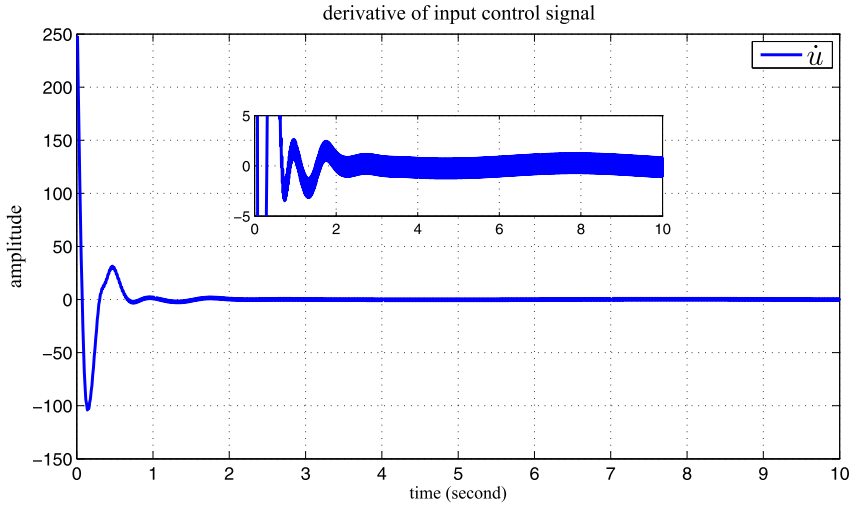

Fig. 21. Derivative of input control signal in DSMC based neural observer.

Simulations have been done by MATLAB with fixed step time of 0.01. The results are shown in Figs. 6–22 for the SMC/DSMC cases. As it can be seen in Figs. 6–8, the system output converges to zero even in the presence of mismatched uncertainty in both SMC and DSMC. Figs. 9–11 (DSMC) show the second state of the system and its estimation. Figs. 12 and 15 for SMC, and 13 and 16 and also 14 and 17 for DSMC show the first and the second sliding surfaces which also converge to zero in finite time. The amplitude of the switching due to the Sign function is very small around these surfaces. Therefore, due to the use of the Sign function in sliding surfaces the invariant property is reserved with respect to both the matched and the mismatched uncertainties. From Figs. 18 (SMC) and 19,20 (DSMC) one can see that the input control signal of the system u and v are smooth and

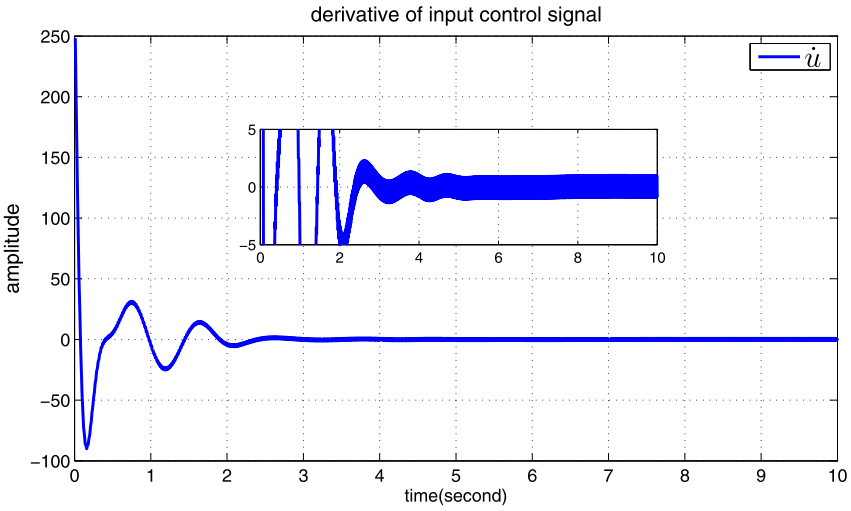

Fig. 22. Derivative of input control signal in DSMC based LTRO.

without switching in DSMC whereas in SMC the chattering can be observed. Refer to Figs. 21 and 22, and note that the initial value of $\dot{u}$ is large but this is not important because the signal $\dot{u}$ is not applied to the system. Finally, by comparison of figures for DSMC approach based neural observer and DSMC approach based LTRO, the good performance of the neural observer with respect to the LTRO can be clearly seen.

Remark 3. Note that in the proposed approach and in the three simulations, all of the system dynamics are considered as the uncertainty (matched or mismatched).

8. Conclusion

In this paper, a new neural observer and a new loop transfer recovery observer (LTRO) with definition of multiple sliding surface and virtual input control signal is proposed. This proposed approach is used to solve the problem of sliding surface estimation in SMC and DSMC. The upper bound of the system uncertainty is not used in SMC, DSMC or in neural observer and in LTRO, which are important in practical applications. Moreover, the invariant property is reserved with respect to the matched and the mismatched uncertainty in the proposed SMC and DSMC. Unlike SMC, in DSMC based proposed methods, the chattering phenomenon can be completely removed. Moreover, from the presented equation one can see the simplicity of DSMC in concept and also in implementation. To have a valid comparison the performance of DSMC is evaluated using two observers: neural observer and LTRO. The presented simulation results shows the favorable features of the neural observer.

References

[1] W. Perruquetti, J.P. Barbot, Sliding Mode Control in Engineering, CRC Press, 2002.
[2] M.-L. Chan, C. Tao, T.-T. Lee, Sliding mode controller for linear systems with mismatched time-varying uncertainties, J. Frankl. Inst. 337 (2–3) (2000) 105–115.
[3] H.-H. Choi, Lmi-based sliding surface design for integral sliding mode control of mismatched uncertain systems, IEEE Trans. Autom. Control 52 (4) (2007) 736–742.

[4] K.-K. Shyu, Y.-W. Tsai, C.-K. Lai, A dynamic output feedback controllers for mismatched uncertain variable structure systems, Automatica 37 (5) (2001) 775–779.
[5] B.-C. Zheng, J.-H. Park, Sliding mode control design for linear systems subject to quantization parameter mismatch, J. Frankl. Inst. 353 (1) (2016) 37–53.
[6] X.-G. Yan, S.K. Spurgeon, C. Edwards, Dynamic sliding mode control for a class of systems with mismatched uncertainty, Eur. J. Control 11 (1) (2005) 1–10.
[7] W. Xiang, F. Chen, An adaptive sliding mode control scheme for a class of chaotic systems with mismatched perturbations and input nonlinearities, Commun. Nonlinear Sci. Numer. Simul. 16 (1) (2011) 1–9.
[8] S. Mondal, C. Mahanta, Chattering free adaptive multivariable sliding mode controller for systems with matched and mismatched uncertainty, ISA Trans. 52 (3) (2013) 335–341.
[9] J. Yang, S. Li, X. Yu, Sliding-mode control for systems with mismatched uncertainties via a disturbance observer, IEEE Trans. Ind. Electron. 60 (1) (2013) 160–169.
[10] J. Yang, J. Su, S. Li, X. Yu, High-order mismatched disturbance compensation for motion control systems via a continuous dynamic sliding-mode approach, IEEE Trans. Ind. Inform. 10 (1) (2014) 604–614.
[11] A. Polyakov, A. Poznyak, Invariant ellipsoid method for minimization of unmatched disturbances effects in sliding mode control, Automatica 47 (7) (2011) 1450–1454.
[12] A.-C. Huang, Y.-C. Chen, Adaptive multiple-surface sliding control for non-autonomous systems with mismatched uncertainties, Automatica 40 (11) (2004) 1939–1945.
[13] Y.-C. Tsai, A.-C. Huang, Fat-based adaptive control for pneumatic servo systems with mismatched uncertainties, Mech. Syst. Signal Process. 22 (6) (2008) 1263–1273.
[14] C.-C. Wen, C.-C. Cheng, Design of sliding surface for mismatched uncertain systems to achieve asymptotical stability, J. Frankl. Inst. 345 (8) (2008) 926–941.
[15] Y. Wang, C. Jiang, D. Zhou, F. Gao, Variable structure control for a class of nonlinear systems with mismatched uncertainties, Appl. Math. Comput. 200 (1) (2008) 387–400.
[16] J. Yang, S. Li, J. Su, X. Yu, Continuous nonsingular terminal sliding mode control for systems with mismatched disturbances, Automatica 49 (7) (2013) 2287–2291.
[17] D. Ginoya, P. Shendge, S. Phadke, Sliding mode control for mismatched uncertain systems using an extended disturbance observer, IEEE Trans. Ind. Electron. 61 (4) (2014) 1983–1992.
[18] D. Ginoya, P. Shendge, S. Phadke, Disturbance observer based sliding mode control of nonlinear mismatched uncertain systems, Commun. Nonlinear Sci. Numer. Simul. 26 (1–3) (2015) 98–107.
[19] F. Li, L. Wu, P. Shi, C.-C. Lim, State estimation and sliding mode control for semi-markovian jump systems with mismatched uncertainties, Automatica 51 (2015) 385–393.
[20] B. Xu, Z. Shi, C. Yang, F. Sun, Composite neural dynamic surface control of a class of uncertain nonlinear systems in strict-feedback form, IEEE Trans. Cybern. 44 (12) (2014) 2626–2634.
[21] X. Li, J. Zhou, A sliding mode control design for mismatched uncertain systems based on states transformation scheme and chattering alleviating scheme, Trans. Inst. Meas. Control 40 (8) (2018) 2509–2516.
[22] B. Xu, F. Sun, Composite intelligent learning control of strict-feedback systems with disturbance, IEEE Trans. Cybern. 48 (2) (2018) 730–741.
[23] B. Xu, Composite learning finite-time control with application to quadrotors, IEEE Trans. Syst., Man, Cybern.: Syst. 13 (99) (2017) 1–10.
[24] J. Wang, C. Shao, Y.Q. Chen, Fractional order sliding mode control via disturbance observer for a class of fractional order systems with mismatched disturbance, Mechatronics 53 (2018) 8–19.
[25] A. Castillo, P. Garca, R. Sanz, P. Albertos, Enhanced extended state observer-based control for systems with mismatched uncertainties and disturbances, ISA Trans. 73 (2018) 1–10.
[26] H. Lee, V.I. Utkin, Chattering suppression methods in sliding mode control systems, Annu. Rev. Control 31 (2) (2007) 179–188.
[27] A. Karami-Mollaee, N. Pariz, H. Shanechi, Position control of servomotors using neural dynamic sliding mode, J. Dyn. Syst., Meas. Control 133 (6) (2011) 061014.
[28] D. Xu, Y. Shi, Z. Ji, Model-free adaptive discrete-time integral sliding-mode-constrained-control for autonomous 4WMV parking systems, IEEE Trans. Ind. Electron. 65 (1) (2018) 834–843.
[29] A. Levant, Sliding order and sliding accuracy in sliding mode control, Int. J. Control 58 (6) (1993) 1247–1263.
[30] G. Bartolini, A. Ferrara, E. Usai, Chattering avoidance by second-order sliding mode control, IEEE Trans. Autom. Control 43 (2) (1998) 241–246.
[31] A. Levant, Robust exact differentiation via sliding mode technique, Automatica 34 (3) (1998) 379–384.
[32] F. Chen, W. Lei, K. Zhang, G. Tao, B. Jiang, A novel nonlinear resilient control for a quadrotor uav via backstepping control and nonlinear disturbance observer, Nonlinear Dyn. 85 (2) (2016) 1281–1295.

[33] Y.-T. Liu, T.-T. Kung, K.-M. Chang, S.-Y. Chen, Observer-based adaptive sliding mode control for pneumatic servo system, Precis. Eng. 37 (3) (2013) 522–530.
[34] Y. Xia, Z. Zhu, M. Fu, Back-stepping sliding mode control for missile systems based on an extended state observer, IET Control Theory Appl. 5 (1) (2011) 93–102.
[35] Q.R. Butt, A.I. Bhatti, M.R. Mufti, M.A. Rizvi, I. Awan, Modeling and online parameter estimation of intake manifold in gasoline engines using sliding mode observer, Simul. Model. Pract. Theory 32 (2013) 138–154.
[36] J. Davila, L. Fridman, A. Levant, Second-order sliding-mode observer for mechanical systems, IEEE Trans. Autom. Control 50 (11) (2005) 1785–1789.
[37] Y. Xiong, M. Saif, Sliding mode observer for nonlinear uncertain systems, IEEE Trans. Autom. Control 46 (12) (2001) 2012–2017.
[38] A. Benchaib, A. Rachid, E. Audrezet, M. Tadjine, Real-time sliding-mode observer and control of an induction motor, IEEE Trans. Ind. Electron. 46 (1) (1999) 128–138.
[39] S. Sonoda, N. Murata, Neural network with unbounded activation functions is universal approximator, Appl. Comput. Harmonic Anal. 43 (2) (2017) 233–268.
[40] D. Tikk, L.T. Kczy, T.D. Gedeon, A survey on universal approximation and its limits in soft computing techniques, Int. J. Approx. Reason. 33 (2) (2003) 185–202.
[41] M. Norgaard, O. Ravn, N. Poulsen, L. Hansen, Neural networks for modelling and control of dynamic systems: a practitioner's handbook, in: Advanced Textbooks in Control and Signal Processing, Springer, Berlin, 2000.
[42] Y. Yang, Y. Yan, Neural network approximation-based nonsingular terminal sliding mode control for trajectory tracking of robotic airships, Aerosp. Sci. Technol. 54 (2016) 192–197.
[43] G. Xu, F. Liu, C. Xiu, L. Sun, C. Liu, Optimization of hysteretic chaotic neural network based on fuzzy sliding mode control, Neurocomputing 189 (2016) 72–79.
[44] Z. Hao, W. Xing-yuan, L. Xiao-hui, Synchronization of complex-valued neural network with sliding mode control, J. Frankl. Inst. 353 (2) (2016) 345–358.
[45] H. Wu, L. Wang, P. Niu, Y. Wang, Global projective synchronization in finite time of nonidentical fractional-order neural networks based on sliding mode control strategy, Neurocomputing 235 (2017) 264–273.
[46] S. Zhou, M. Chen, C.-J. Ong, P.C. Chen, Adaptive neural network control of uncertain mimo nonlinear systems with input saturation, Neural Comput. Appl. 27 (5) (2016) 1317–1325.
[47] T. Sun, H. Pei, Y. Pan, H. Zhou, C. Zhang, Neural network-based sliding mode adaptive control for robot manipulators, Neurocomputing 74 (14–15) (2011) 2377–2384.
[48] D. Lin, X. Wang, Observer-based decentralized fuzzy neural sliding mode control for interconnected unknown chaotic systems via network structure adaptation, Fuzzy Sets Syst. 161 (15) (2010) 2066–2080.
[49] S. Frikha, M. Djemel, N. Derbel, Observer based adaptive neuro-sliding mode control for MIMO nonlinear systems, Int. J. Control, Autom. Syst. 8 (2) (2010) 257–265.
[50] M.T. Andani, Z. Ramezani, S. Moazami, J. Cao, M.M. Arefi, H. Zargarzadeh, Observer-based sliding mode control for path tracking of a spherical robot, Complexity 2018 (2018).
[51] X. Guo, W. Yan, R. Cui, Neural network-based nonlinear sliding-mode control for an AUV without velocity measurements, Int. J. Control 92 (3) (2019) 677–692.
[52] D. Xu, J. Liu, X.G. Yan, W. Yan, A novel adaptive neural network constrained control for a multi-area interconnected power system with hybrid energy storage, IEEE Trans. Ind. Electron. 65 (8) (2018) 6625–6634.
[53] J.-J.E. Slotine, W. Li, Applied Nonlinear Control, Prentice hall, Englewood Cliffs, NJ, 1991.
[54] M.K. Sifakis, S.J. Elliott, Strategies for the control of chaos in a duffing–holmes oscillator, Mech. Syst. Signal Process. 14 (6) (2000) 987–1002.
[55] W. Li, T. Lan, W. Lin, Adaptive tracking control of duffing-holmes chaotic systems with uncertainty, in: IEEE 5th International Conference on Computer Science & Education (ICCSE), 2010, pp. 1193–1197.
[56] J.C. Doyle, G. Stein, Robustness with observers, IEEE Trans. Autom. Control 24 (1979) 607–611.